Title	In silico non-linear dynamic analysis reflecting in vitro physical properties of CAD/CAM resin composite blocks
Author(s)	Karaer, Oğuzcan; Yamaguchi, Satoshi; Nakase, Yutaro et al.
Citation	Journal of the Mechanical Behavior of Biomedical Materials. 2020, 104, p. 103697
Version Type	AM
URL	https://hdl.handle.net/11094/93084
rights	©2020. This manuscript version is made available under the CC-BY-NC-ND 4.0 license https://creativecommons.org/licenses/by-nc-nd/4.0/
Note	

1   Research paper

2

3   *In silico* **non-liner dynamic analysis reflecting** *in vitro* **physical properties of CAD/CAM**

4   **resin composite blocks**

5

6   Dr. Oğuzcan Karaer[a], DDS, Dr. Satoshi Yamaguchi[b]*, Ph.D., Dr. Yutaro Nakase[b,c], DDS, Dr.

7   Chunwoo Lee[b], DDS, Prof. Satoshi Imazato[b, d], DDS, Ph.D.

8

9   [a] Department of Prosthodontics, Faculty of Dentistry, Ankara University, Ankara 06560,

10   Turkey

11   [b] Department of Biomaterials Science, Osaka University Graduate School of Dentistry, 1-8

12   Yamadaoka, Suita, Osaka 565-0871, Japan

13   [c] Department of Pediatric Dentistry, Osaka University Graduate School of Dentistry, 1-8

14   Yamadaoka, Suita, Osaka 565-0871, Japan

15   [d] Department of Advanced Functional Materials Science, Osaka University Graduate School

16   of Dentistry, 1-8 Yamadaoka, Suita, Osaka 565-0871, Japan

17

18

19   * Correspondence should be addressed to Satoshi Yamaguchi

20   Department of Biomaterials Science, Osaka University Graduate School of Dentistry

21   1-8 Yamadaoka, Suita, Osaka 565-0871, Japan

22   Tel/Fax: +81-6-6879-2917

23   E-mail: yamagu@dent.osaka-u.ac.jp

24

25

26

27   **Abbreviations**

28   CAD/CAM   Computer-aided design/computer-aided manufacturing

29   NTP   Notchless triangular prism

30   FEA   Finite element analysis

31   SEM   Scanning electron microscopy

32

33

34   **ABSTRACT**

35   ***Purpose.*** The aim of this study was to assess the validity of *in silico* models of three-point

36   bending tests to reflect *in vitro* physical properties obtained from three commercially

37   available computer-aided design/computer-aided manufacturing (CAD/CAM) resin composite

38   blocks and demonstrate notchless triangular prism analysis with those properties.

39   ***Material and Methods.*** Three types of commercially available CAD/CAM resin composite

40   blocks were used: Cerasmart 300 (CS300; GC, Tokyo, Japan), Katana Avencia P Block (AP;

41   Kuraray Noritake Dental, Tokyo, Japan), and KZR CAD HR3 Gamma Theta (GT; Yamakin,

42   Osaka, Japan). *In vitro/in silico* three-point bending tests were conducted to obtain elastic

43   modulus and fracture strain for nonlinear dynamic finite element analysis (n=10/each).

44   Fractured surfaces of specimens after *in vitro* NTP tests were observed, and the fracture

45   toughness of each CAD/CAM resin composite was obtained by *in silico* NTP analysis.

46   ***Results.*** Both *in vitro* and *in silico* load–displacement curves obtained from three-point

47   bending tests were significantly correlated ($p < 0.05$). The elastic moduli of CS300, AP, and

48   GT were 8.0 GPa, 10.0 GPa, and 9.0 GPa, respectively. The fracture toughness values

49   obtained from *in silico* NTP analysis of CS300, AP, and GT were 5.057 MPa·m$^{1/2}$, 4.193

50   MPa·m$^{1/2}$, and 4.880 MPa·m$^{1/2}$, respectively. There was no significant difference in the length

51   of the stable region among the three CAD/CAM resin composites ($p = 0.09$).

52   ***Conclusions.*** The *in silico* approach established in this study showed acceptable reflection of

53   *in vitro* physical properties and will be useful for assessing fracture toughness related to the

54   longevity of CAD/CAM resin composites without wastage of materials.

55

56   **KEYWORDS**: Resin composites, Fracture toughness, Finite element analysis, Computer

57   aided design, Computer aided manufacturing

58

1. INTRODUCTION

Computer-aided design/computer-aided manufacturing (CAD/CAM) resin composite blocks are esthetic restorative materials and may possibly be used as an alternative to metals or ceramics (Ruse and Sadoun, 2014). CAD/CAM resin composite blocks have greater mechanical properties than conventional filling resin composites because of their highly dense nanofillers (Coldea et al., 2013a, b; Okada et al., 2014) and pre-polymerization procedures (Nguyen et al., 2012, 2013). After approval by Japanese health insurance companies in 2014, clinical treatment with CAD/CAM resin composites in the molar region have steadily increased. However, the longevity of CAD/CAM resin composite molar crowns is still unknown (Yamaguchi et al., 2018a).

The fracture toughness of resin composites is one key criterion for evaluating resistance to crack propagation from the existing initiation points related to the fatigue performance of CAD/CAM resin composites. Additionally, a significant weak correlation between wear performance and clinical fractures relating to the fracture toughness has been reported (Heintze et al., 2017). The single-edge notched beam and the chevron notch short rod/beam tests are available to evaluate the fracture toughness of dental materials (Fujishima and Ferracane, 1996; Ilie et al., 2012; Ornaghi et al., 2014; Tantbirojn et al., 2003). However, it is difficult to reproduce the shape of the notch, making the specimen preparation challenging.

77   Notchless triangular prism (NTP) tests have been proposed by Ruse *et al*. (Ruse et al.,

78 1996) as a simpler method to evaluate both the fracture toughness of materials and bonded

79 interfaces between the adhesive and restorative materials (Eldafrawy et al., 2018; Mesmar and

80 Ruse, 2019). Tensile stress calculated by finite element analysis (FEA) using the NTP test and

81 the chevron notch short rod test showed no differences in distribution (Ruse et al., 1996).

82   FEA is well established as a method for assessing stress distribution, and is useful for

83 investigating fracture initiation points in dental materials (Ausiello et al., 2004; Coelho et al.,

84 2008; Dal Piva et al., 2018; Della Bona et al., 2013; Yamaguchi et al., 2018a; Yamanishi et al.,

85 2014). It is difficult to determine which is the best composition of CAD/CAM resin composites

86 to optimize fracture toughness, and *in vitro* fracture toughness tests are still conducted by using

87 actual specimens. *In vitro* experimental results involve complex factors such as shape, size,

88 materials, layout of fillers, and coupling conditions between fillers and the resin matrix

89 (Ferracane, 2011). One of the advantages of FEA is the ability to evaluate the stress distribution

90 focusing on specific factors related to mechanical performance (Yamaguchi et al., 2017). This

91 feature makes FEA a particularly useful tool in materials design.

92   Non-linear dynamic FEA can represent fracture propagation corresponding to the

93 fracture criteria of materials, as well as the stress distributions (Yamaguchi et al., 2014).

94 Fracture criteria are important factors for obtaining accurate fracture loads reflecting the *in vitro*

95   results. The maximum principal strain has been reported as the best fracture criterion for

96   evaluating the flexural strength of resin composites (Yamaguchi et al., 2018b). The combination

97   of nonlinear dynamic FEA and the fracture criterion makes it possible to develop *in silico*

98   models of NTP tests to reflect the *in vitro* results.

99   The aim of this study was to assess the validity of *in silico* models of three-point bending

100 tests to reflect *in vitro* physical properties obtained from three commercially available

101 CAD/CAM resin composite blocks and demonstrate notchless triangular prism analysis with

102 those properties.

2. Materials and methods

2.1 CAD/CAM resin composites blocks

Three types of commercially available CAD/CAM resin composites blocks were used:

Cerasmart 300 (CS300; GC, Tokyo, Japan), Katana Avencia P Block (AP; Kuraray Noritake

Dental, Niigata, Japan), and KZR CAD HR3 Gamma Theta (GT; Yamakin, Osaka, Japan).

Details of the material composition of each block are summarized in Table 1.

Table 1. Composition of CAD/CAM resin composites used in this study

	Code	Manufacturer	Filler and monomer	Filler content (wt%)
Cerasmart 300	CS300	GC	Barium glass, silica powder UDMA, Bis-MEPP, polyfunctional methacrylate	78
Katana Avencia P Block	AP	Kuraray Noritake Dental	Mixed filler with silanated barium glass, silanated colloidal silica, Cured resins consisting of methacrylate monomer, UDMA	82
KZR-CAD HR3 Gamma Theta	GT	YAMAKIN	Inorganic oxide filler, fluoride-releasing filler, spherical nanofiller (SiO_2) Methacrylate monomer	75

2.2 *In vitro*/*in silico* three-point bending tests

In vitro three-point bending tests were conducted using each material ($4.0 \times 1.2 \times 14.0$

mm specimen, n = 10) after storage in water for 24 hours using a universal testing machine

(EZ-SX, Shimadzu, Kyoto, Japan) with a 1.0 mm/min cross head speed. The obtained load–

displacement curve was converted into a stress–strain curve. The flexural modulus was obtained

from the initial slope of the stress–strain curve, and the fracture strain was recorded at the end

117   of the curve. Micro computed tomography (micro-CT; R_mCT2, Rigaku, Tokyo, Japan)

118   analysis for calculating the volume and the weight measurement of each specimen were

119   conducted to calculate densities. Using the data obtained by these *in vitro* tests, the elastic

120   modulus of each material was obtained by *in silico* non-linear dynamic FEA (LS-DYNA, LSTC,

121   Livermore, CA, USA). The flexural modulus and the elastic modulus are not equal. The flexural

122   modulus was used as an initial elastic modulus for three-point bending analysis. After the first

123   analysis, there is some difference between *in vitro* and *in silico* load displacement curve. Until

124   converging those curves, the analysis was repeatedly conducted. Finally, the elastic modulus of

125   each material was determined. The Poisson's ratio of each material was set to 0.38 according

126   to that of dental composites (Greaves et al., 2011).

127

128   **2.3   Specimen preparation and *in vitro* notchless triangular prism tests**

129   For the notchless triangular prism (NTP) test, 6 × 6 × 6 × 12 mm specimens were

130   prepared by milling machine (DWX-51D, Roland DG, Hamamatsu, Japan) and polished with

131   #2000 SiC paper. All the specimens were immersed into 37ºC water for 24 hours. A fracture

132   initiation point 0.1 mm in depth was opened on the middle edge of the triangular prism

133   specimen using a stainless steel razor blade using custom-made jigs (TRUE SEED, Kyoto,

134   Japan). The edge of the triangular specimens was carefully observed under an optical

135 microscope (HM-211, Mitsutoyo, Kawasaki, Japan) with $10\times$ magnification. The specimens

136 were wiped and fixed on custom-made jigs for the NTP tests (TRUE SEED). The NTP tests

137 were conducted with a universal testing machine (EZ-SX, Shimadzu, Kyoto, Japan) with a 1.0

138 mm/min crosshead speed.

139

140 　　　The fractured surfaces of the specimens were then gold-coated using Quick Coater (SC-

141 701, Sanyu Electron, Tokyo, Japan) and observed by scanning electron microscopy (SEM;

142 JSM-6390BU, JEOL, Tokyo, Japan) under $30\times$ magnification at 5 kV. The length from the

143 crack initiation point to the boundary between the stable and unstable regions was measured

144 using Image J software (National Institute of Health, Bethesda, MD, USA).

145

146 **2.4　*In silico* notchless triangular prism analysis**

147 　　　Using the elastic moduli and fracture strains obtained from *in vitro* three-point bending

148 tests and densities, NTP analysis was conducted by *in silico* non-linear dynamic FEA using the

149 same CAD models designed for the custom-made jigs for the NTP tests (Fig. 1). The fracture

150 toughness (K_{1c}) of each model was calculated using the following equation:
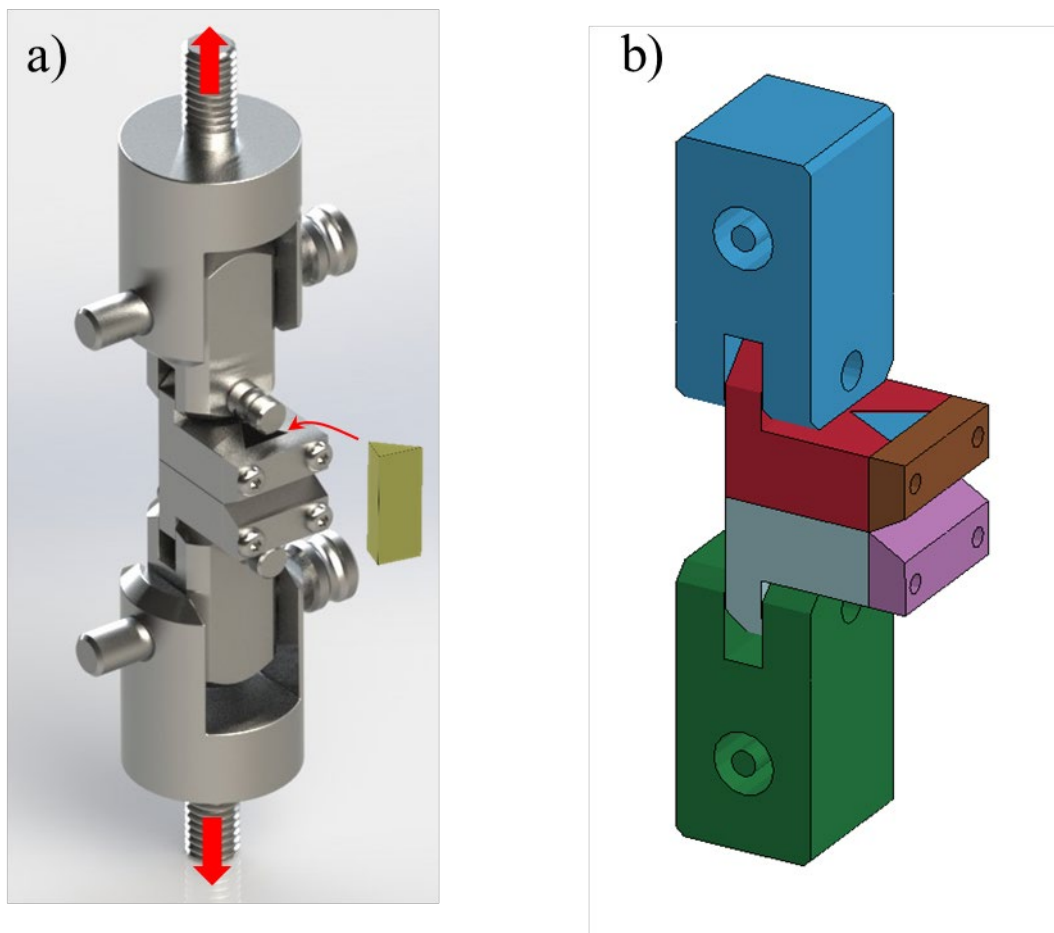
151

152
$$K_{1C} = \frac{P}{D\sqrt{W}} Y_{\min},$$

153

154   where P is the load at fracture, D (12.0 mm) is the length of the prism, W (10.5 mm) is the

155   length of the mold, and Y_{min} (28.0) is the stress intensity factor.

156   The maximum principal strain distribution was obtained once there was 0.1 mm displacement

157   until fracture.

158

159

160   **Fig. 1** CAD models for NTP tests. **a** CAD models of *in vitro* NTP tests for fabricating custom-

161   made jigs. **b** CAD models for *in silico* NTP analysis.

162

163 **2.5   Statistical analysis**

164   Loads at each time point obtained from the *in vitro* three-point bending tests were

165 compared statistically with the value determined by *in silico* analysis using Pearson's

166 correlation tests (PASW Statistics 18, IBM, Somers, NY, USA). Additionally, loads at each

167 time point obtained from the *in vitro* NTP tests were compared statistically with the value

168 determined by *in silico* analysis using Spearman's correlation test.

169   The lengths of stable region obtained from the SEM images were compared statistically

170 using one-way analysis of variance (ANOVA) with Tukey's post hoc test.

171   *P*-values of less than 0.05 were considered as statistically significant for all tests.

172

173 **3. RESULTS**

174 **3.1 Elastic moduli obtained from *in silico* three-point bending analysis**

175 The flexural moduli, densities, and fracture strains of CS300, AP, and GT are

176 summarized in Table 2. *In vitro* / *in silico* load–displacement curves after the three-point

177 bending tests/analysis are shown in Figure 2. The *in vitro* curve was obtained by averaging all

178 loads at each time point. Both *in vitro* and *in silico* load–displacement curves were significantly

179 correlated (CS300: R=0.99, AP: R=1.0, GT: R=0.99, $p < 0.05$). The elastic moduli of CS300,

180 AP, and GT were 8.0 GPa, 10.0 GPa, and 9.0 GPa, respectively.

181

Table 2. Physical properties of CAD/CAM resin composites obtained by *in vitro* three-point bending tests, micro-CT analysis, and weight measurement

	Flexural modulus (GPa)	Density (g/cm^3)	Fracture strain (ε)
CS300	6.765 ± 1.042	2.17 ± 0.00682	0.0366 ± 0.00627
AP	9.261 ± 1.774	2.35 ± 0.00994	0.0247 ± 0.00267
GT	7.424 ± 1.053	2.08 ± 0.00364	0.0322 ± 0.00346

182

a)

183

b)

184

185

186
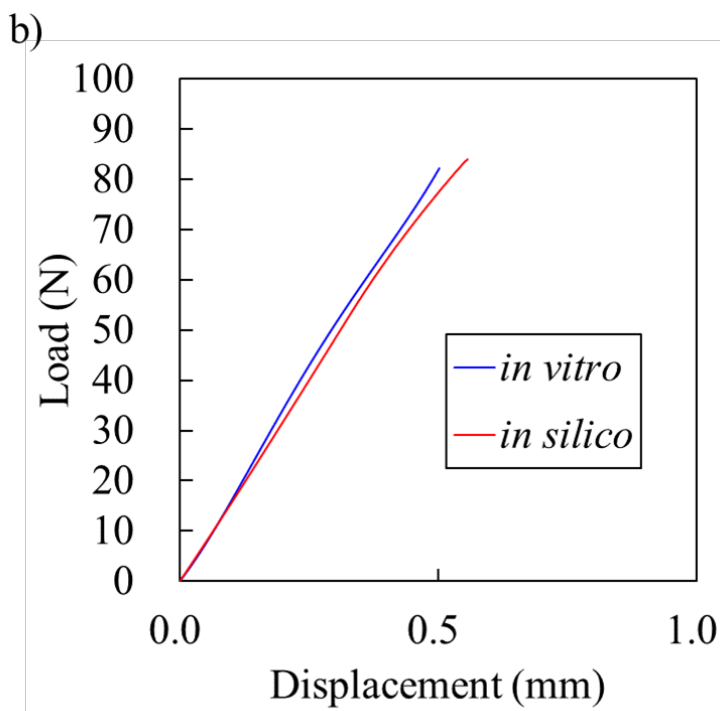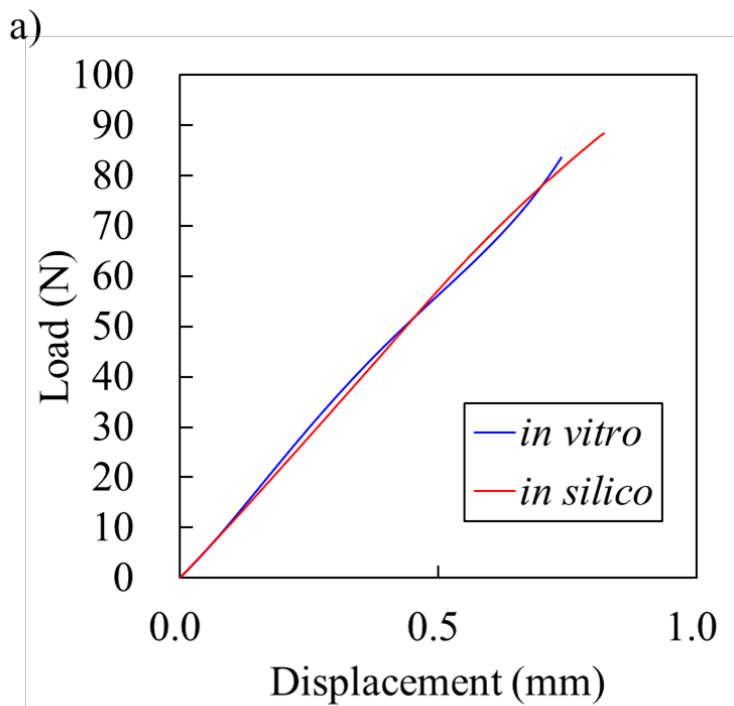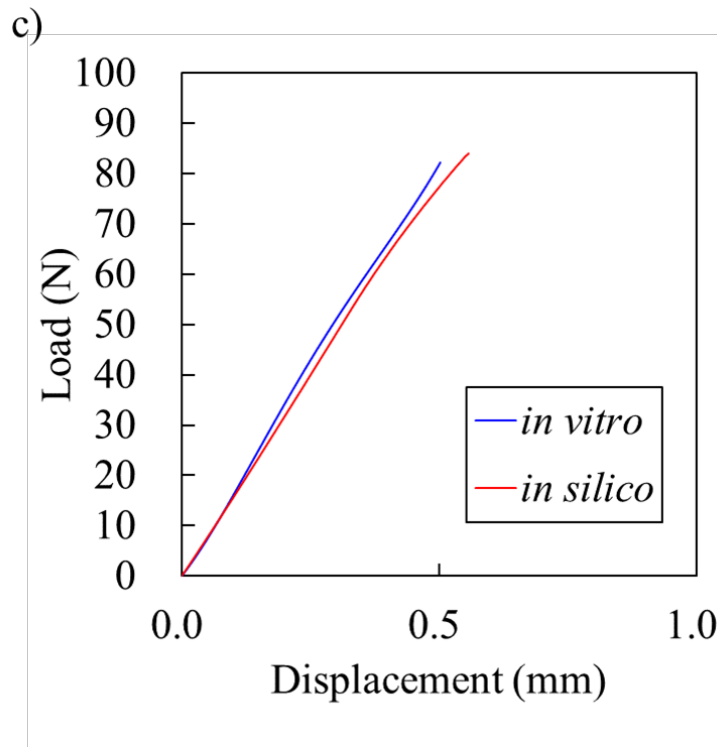
Fig. 2 Load–displacement curve obtained from *in vitro* / *in silico* three-point bending tests. The

in vitro curve was obtained by averaging all curves. **a** CS300, **b** AP, **c** GT.

3.2 Fracture toughness after *in silico* NTP analysis

The fracture toughness values of CS300, AP, and GT obtained in *in silico* NTP analysis

were 5.057 MPa·m$^{1/2}$, 4.193 MPa·m$^{1/2}$, and 4.880 MPa·m$^{1/2}$, respectively. *In silico* load–

displacement curves of CS300, AP, and GT obtained in *in silico* NTP analysis are shown in

Figure 3. The *in vitro* curve was obtained by averaging all loads at each time point. Both *in*

vitro and *in silico* load–displacement curves were significantly correlated (CS300: R=1.0, AP:

R=1.0, GT: R=1.0, $p < 0.05$).

197

198
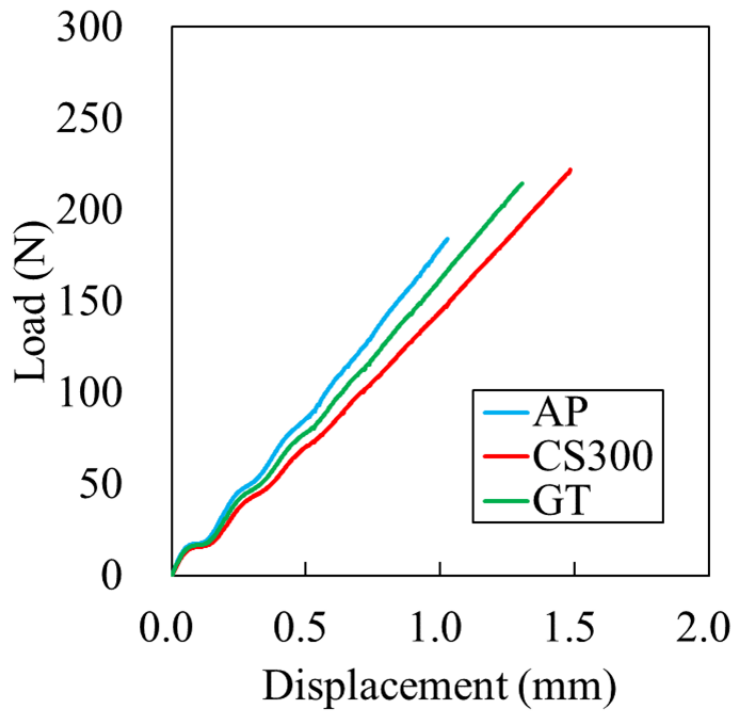
Fig. 3 Load–displacement curves obtained from *in silico* NTP analysis.

200

201 **3.3   Fractographic analysis**

202   Figure 4 shows SEM images at one side of the fractured surface from the initiation point

203 after NTP tests for CS300 (Fig. 4a), AP (Fig. 4b), and GT (Fig. 4c). White arrows and bold
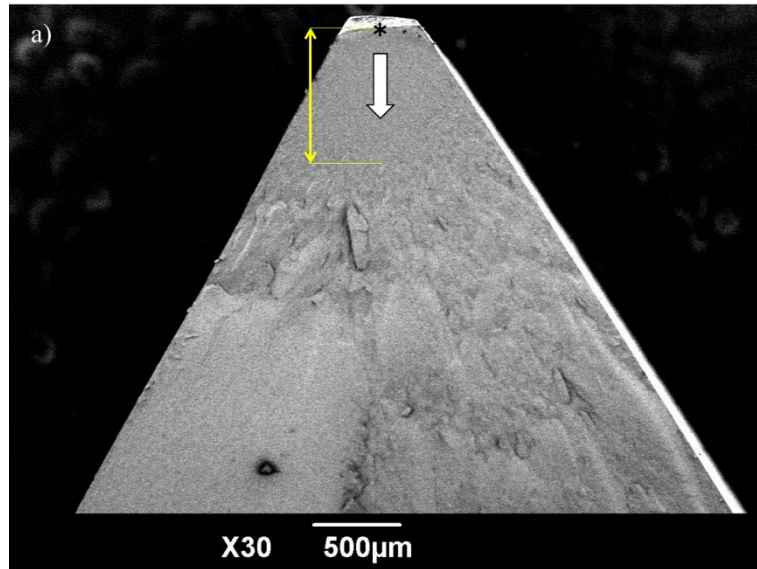
204 white arrows indicate crack initiation points and the direction of crack propagation. Stable and

205 unstable areas are indicated by yellow lines and were observed throughout the fracture surface
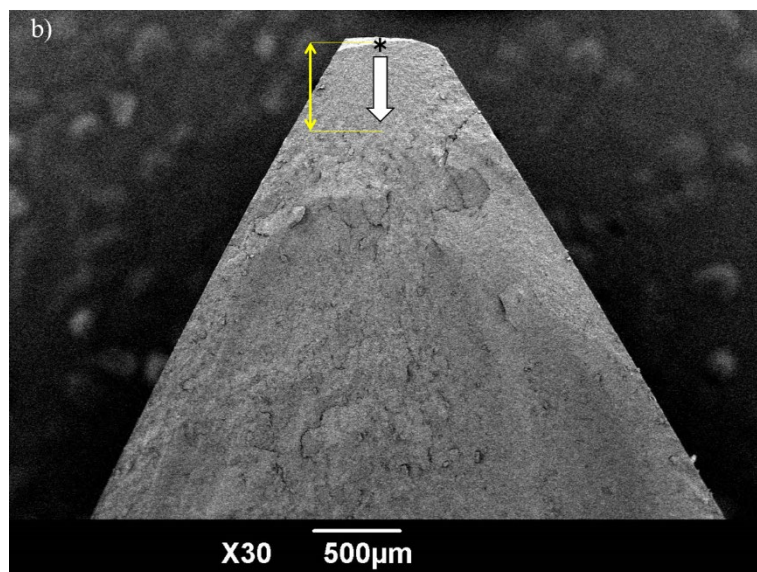
206 of the specimens. The means and standard deviations of the length of the stable region are

207   shown in Figure 5. There was no significant difference among the three CAD/CAM resin
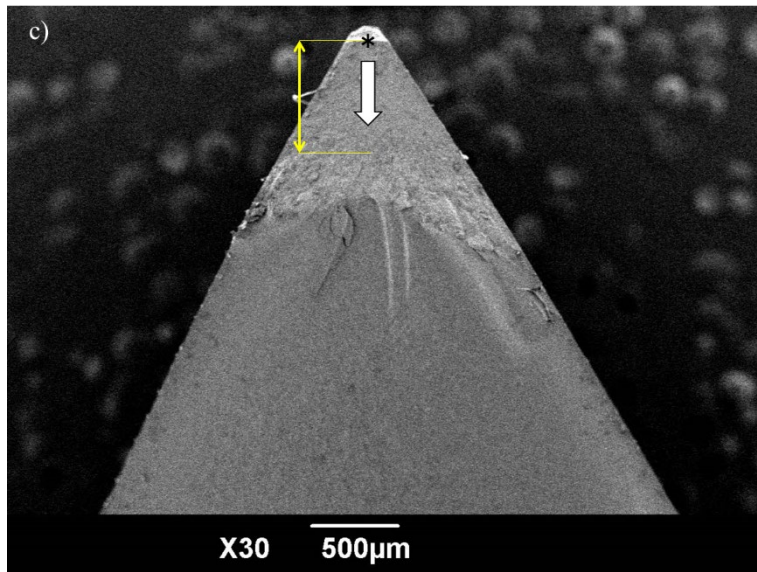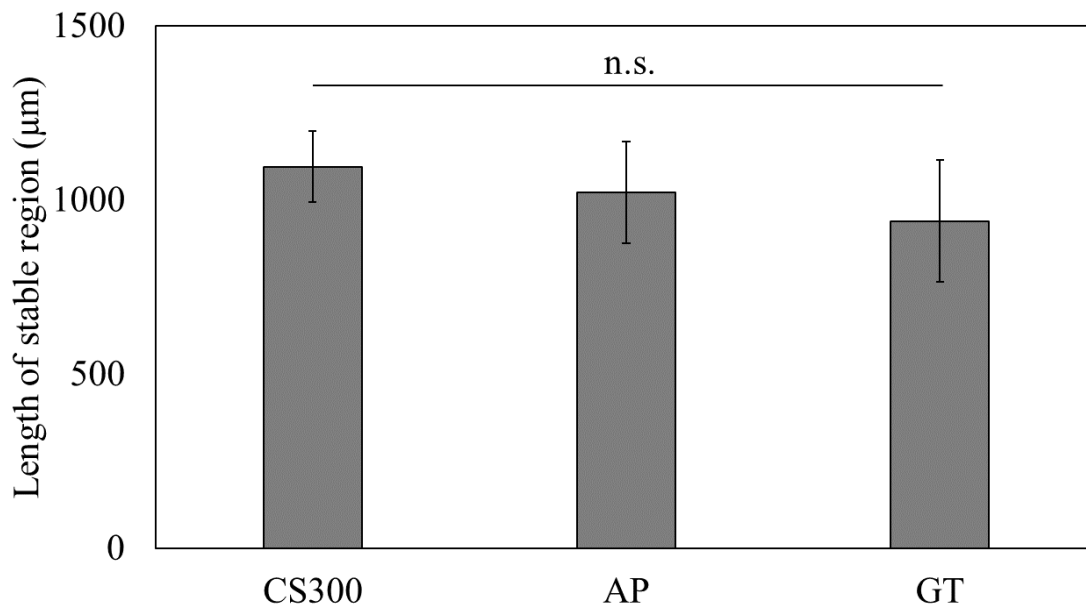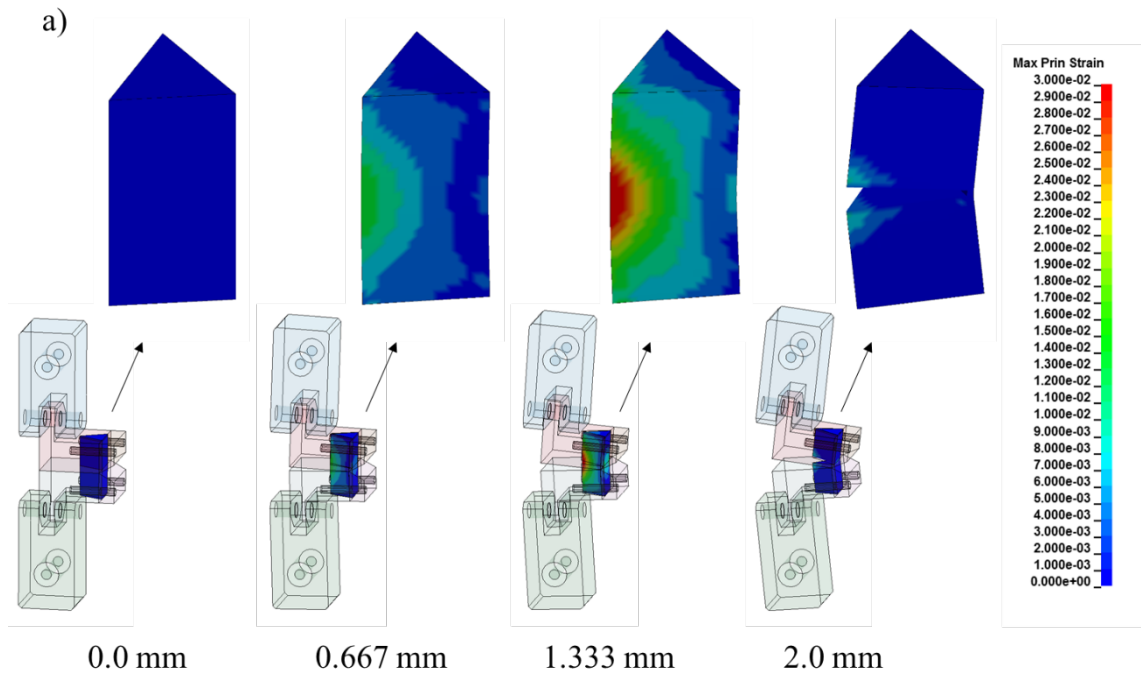
208   composites ($p = 0.09$).

209

210

211

212

213 **Fig. 4** SEM images of fractured surface of specimens after *in vitro* NTP tests. The yellow arrows

214 indicate the length of the stable region. The black asterisks indicate the fracture initiation point.

215 The white arrows indicate the direction of crack propagation. **a** CS300, **b** AP, **c** GT.
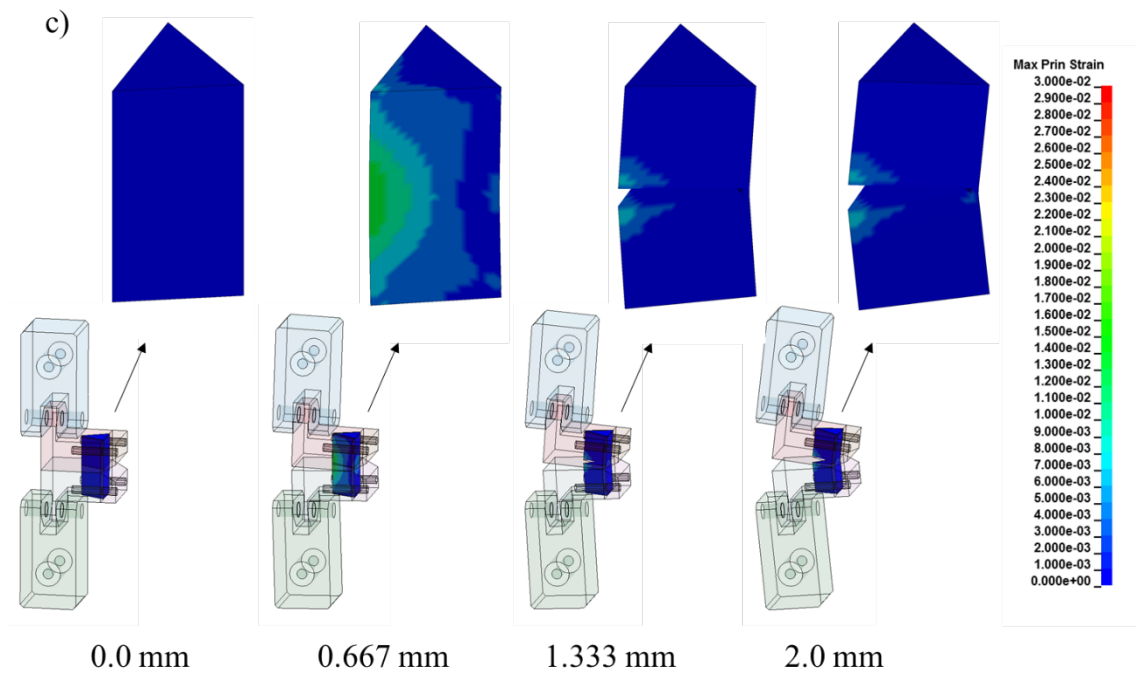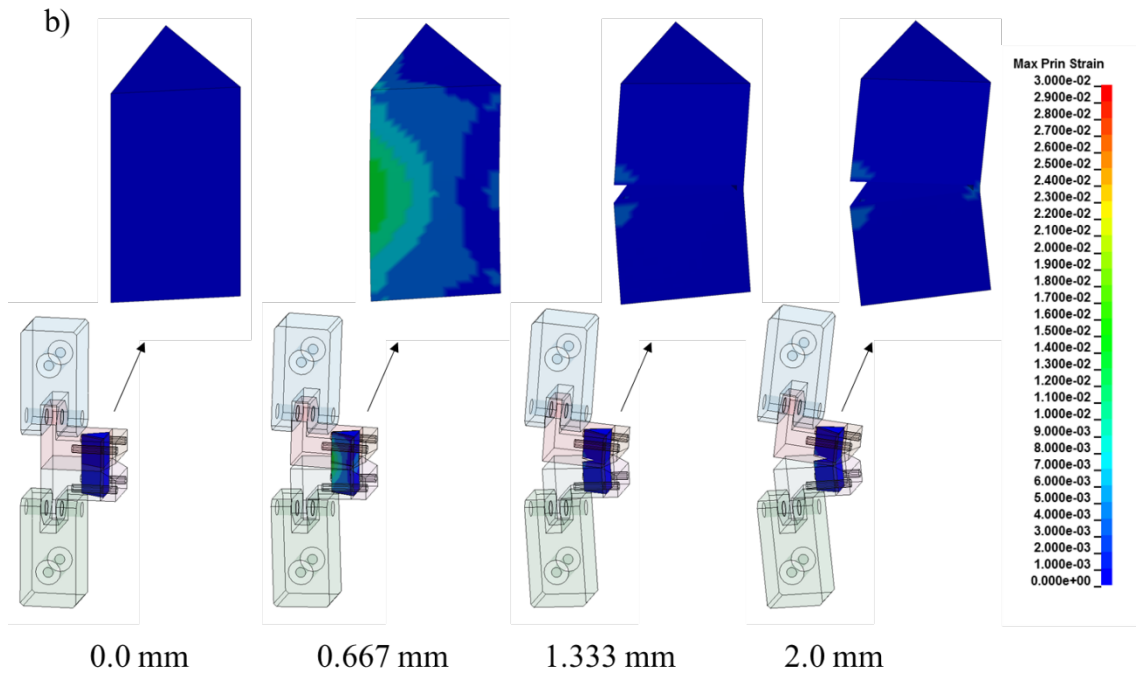
216

217

218 **Fig. 5** Length of the stable region on the fracture surface after *in vitro* NTP tests.

219

220 **3.4   Maximum principal strain distribution in the specimens**

221   Figure 6 shows the maximum principal strain distribution during deformation and after

222 fracture for CS300 (Fig. 6a), AP (Fig. 6b), and GT (Fig. 6c). The tensile strain (positive value

223 of maximum principal strain) is concentrated on the middle edge of the specimens. Fracture

224 was observed at the stretch after exceeding the fracture strain of each material.

a)

| 0.0 mm | 0.667 mm | 1.333 mm | 2.0 mm |

225

b)

0.0 mm   0.667 mm   1.333 mm   2.0 mm

226

c)

0.0 mm   0.667 mm   1.333 mm   2.0 mm

227

Fig. 6 Maximum principal strain distribution at each calculation point. 0.0 mm, 0.667 mm,

1.333 mm, and 2.0 mm from left to right. **a** CS300, **b** AP, **c** GT.

4. DISCUSSION

An *in silico* three-point bending model was successfully developed and could be used to predict fracture toughness to reflect *in vitro* physical properties obtained from three commercially available CAD/CAM resin composite blocks and demonstrate *in silico* notchless triangular prism (NTP) analysis with those properties. We believe that the *in silico* approach using non-linear dynamic FEA established in this study will become an alternative way to assess fracture toughness related to the longevity of CAD/CAM resin composite crowns without wastage of materials.

The three-point bending tests indicated that the elastic moduli of CS300 and GT were lower than that of AP. From the composition of the materials as shown in Table 1, the inorganic filler content of CS300 and GT was 78 wt% and 75 wt%, respectively, while that of AP was 82 wt%. A lower filler content of resin composites results in a lower flexural modulus (Randolph et al., 2016)/strength (Yamaguchi et al., 2018b) and the volume of the matrix resins must be increased in relation to the amount of fillers. Thus, the lower filler content of CS300 and GT may have resulted in a lower elastic modulus. The elastic modulus is one of the mechanical properties used for evaluating and ranking resin composites (Ilie et al., 2017), and is defined as the initial slope of the stress–strain curve for a given material under loading.

249   *In silico* three-point bending analysis using non-linear dynamic FEA successfully

250   reflected the *in vitro* testing results. These results suggest that the elastic modulus, density, and

251   fracture strain of each CAD/CAM resin composite could be useful for predicting the flexural

252   modulus and flexural strength. These parameters may be applied to other testing methods such

253   as biaxial flexural tests, four-point bending tests, and fracture toughness tests such as the NTP

254   tests used in this study.

255   Fracture toughness is an intrinsic material property and is a measure of the energy

256   required to propagate a crack from an existing defect. The NTP test for evaluating fracture

257   toughness adopted in this study was originally proposed by Ruse *et al.* (Ruse et al., 1996). The

258   applications of NTP tests are now expanding to evaluate the interfacial properties of dental

259   materials (Alkadi and Ruse, 2016; Eldafrawy et al., 2018; Mesmar and Ruse, 2019). The *in*

260   *silico* load–displacement curve of GT in the NTP tests was well matched to the *in vitro* curve.

261   For CS300 and AP, lower fracture loads and displacements were observed *in vitro* compared

262   with *in silico* with statistically significant correlations. One of the reasons for these differences

263   was the construction of jigs for the NTP tests. The specimen cannot be fixed to the jigs without

264   fixation jigs with screws. Even if there are slight differences in the specimen's dimensions at

265   the microscale order, static and dynamic friction properties among the jigs and the specimen

266   will be dramatically changed on the fixation force. Thus, the *in silico* approach could avoid

267   these frictional effects and allow direct comparison by focusing on the different material

268   composition of each CAD/CAM resin composite block.

269   The SEM images showed that both stable and unstable areas (Alkadi and Ruse, 2016)

270   resulted in mode I fracture (the tensile loading direction is vertical to the fracture surface). The

271   length of the stable area from the crack initiation point to the boundary between the stable and

272   unstable areas was not significantly different among the CAD/CAM resin composites, while a

273   shorter length of stable area has been reported in lithium disilicate glass ceramics (Alkadi and

274   Ruse, 2016; Mesmar and Ruse, 2019). These results suggest that CAD/CAM resin composites

275   inhibit crack propagation to a greater degree than lithium disilicate glass ceramics.

276   Stable and unstable areas were not observable on the *in silico* models because the mesh

277   size of 0.3 mm was too large to represent the nano/microstructural details of the fractured

278   surface. The calculation cost would need to be increased corresponding to a higher resolution

279   mesh. Multi-scale analysis may be helpful to find the crack initiation point at the

280   nano/microscale level (Takano et al., 2010; Takano et al., 2003; Yamaguchi et al., 2017). *In*

281   *silico* nanoscale models of CAD/CAM resin composites blocks have been developed using

282   electron microscopy with cryo-stage and focused ion beam (Lee et al., 2019). The combination

283   of non-linear dynamic FEA and multi-scale analysis using nanoscale models may accelerate

284   elucidation of the fracture mechanism and the development of new materials with greater

285   longevity.

286   While of CAD/CAM resin composites exhibit greater fracture toughness, hydrolysis of

287   the silane coupling and matrix resins in the oral environment (Drummond, 2008; Kusuma

288   Yulianto et al., 2019) should be considered in future studies. Nanoscale models containing a

289   silane coupling layer are under development for investigating the influence on the mechanical

290   properties of CAD/CAM resin composites.

291

5. CONCLUSIONS

292

293   The *in silico* approach established in this study acceptably reflected the *in vitro* physical

294   properties and will be useful for assessing fracture toughness related to the longevity of

295   CAD/CAM resin composites without wastage of materials.

296

ACKNOWLEDGEMENTS

302

REFERENCES

Alkadi, L., Ruse, N.D., 2016. Fracture toughness of two lithium disilicate dental glass ceramics.

J Prosthet Dent 116, 591-596.

Ausiello, P., Rengo, S., Davidson, C.L., Watts, D.C., 2004. Stress distributions in adhesively

cemented ceramic and resin-composite Class II inlay restorations: a 3D-FEA study. Dent Mater

20, 862-872.

Coelho, P.G., Calamia, C., Harsono, M., Thompson, V.P., Silva, N.R., 2008. Laboratory and

FEA evaluation of dentin-to-composite bonding as a function adhesive layer thickness. Dent

Mater 24, 1297-1303.

Coldea, A., Swain, M.V., Thiel, N., 2013a. In-vitro strength degradation of dental ceramics and

novel PICN material by sharp indentation. J Mech Behav Biomed Mater 26, 34-42.

Coldea, A., Swain, M.V., Thiel, N., 2013b. Mechanical properties of polymer-infiltrated-

ceramic-network materials. Dent Mater 29, 419-426.

Dal Piva, A.M.O., Tribst, J.P.M., Borges, A.L.S., Souza, R., Bottino, M.A., 2018. CAD-FEA

modeling and analysis of different full crown monolithic restorations. Dent Mater 34, 1342-

1350.

Della Bona, A., Borba, M., Benetti, P., Duan, Y., Griggs, J.A., 2013. Three-dimensional finite

element modelling of all-ceramic restorations based on micro-CT. J Dent 41, 412-419.

321   Drummond, J.L., 2008. Degradation, fatigue, and failure of resin dental composite materials. J

322   Dent Res 87, 710-719.

323   Eldafrawy, M., Ebroin, M.G., Gailly, P.A., Nguyen, J.F., Sadoun, M.J., Mainjot, A.K., 2018.

324   Bonding to CAD-CAM Composites: An Interfacial Fracture Toughness Approach. J Dent Res

325   97, 60-67.

326   Ferracane, J.L., 2011. Resin composite--state of the art. Dent Mater 27, 29-38.

327   Fujishima, A., Ferracane, J.L., 1996. Comparison of four modes of fracture toughness testing

328   for dental composites. Dent Mater 12, 38-43.

329   Greaves, G.N., Greer, A.L., Lakes, R.S., Rouxel, T., 2011. Poisson's ratio and modern materials.

330   Nat Mater 10, 823-837.

331   Heintze, S.D., Ilie, N., Hickel, R., Reis, A., Loguercio, A., Rousson, V., 2017. Laboratory

332   mechanical parameters of composite resins and their relation to fractures and wear in clinical

333   trials-A systematic review. Dent Mater 33, e101-e114.

334   Ilie, N., Hickel, R., Valceanu, A.S., Huth, K.C., 2012. Fracture toughness of dental restorative

335   materials. Clin Oral Investig 16, 489-498.

336   Ilie, N., Hilton, T.J., Heintze, S.D., Hickel, R., Watts, D.C., Silikas, N., Stansbury, J.W.,

337   Cadenaro, M., Ferracane, J.L., 2017. Academy of Dental Materials guidance-Resin composites:

338   Part I-Mechanical properties. Dent Mater 33, 880-894.

339   Kusuma Yulianto, H.D., Rinastiti, M., Cune, M.S., de Haan-Visser, W., Atema-Smit, J.,

340   Busscher, H.J., van der Mei, H.C., 2019. Biofilm composition and composite degradation

341   during intra-oral wear. Dent Mater.

342   Lee, C., Yamaguchi, S., Ohta, K., Imazato, S., 2019. Mechanical properties of computer-aided

343   design/computer-aided manufacturing resin composites assuming perfect silane coupling using

344   in silico homogenization of cryo-electron microscopy images. J Prosthodont Res 63, 90-94.

345   Mesmar, S., Ruse, N.D., 2019. Interfacial Fracture Toughness of Adhesive Resin Cement-

346   Lithium-Disilicate/Resin-Composite Blocks. J Prosthodont 28, e243-e251.

347   Nguyen, J.F., Migonney, V., Ruse, N.D., Sadoun, M., 2012. Resin composite blocks via high-

348   pressure high-temperature polymerization. Dent Mater 28, 529-534.

349   Nguyen, J.F., Migonney, V., Ruse, N.D., Sadoun, M., 2013. Properties of experimental

350   urethane dimethacrylate-based dental resin composite blocks obtained via thermo-

351   polymerization under high pressure. Dent Mater 29, 535-541.

352   Okada, K., Kameya, T., Ishino, H., Hayakawa, T., 2014. A novel technique for preparing dental

353   CAD/CAM composite resin blocks using the filler press and monomer infiltration method. Dent

354   Mater J 33, 203-209.

355   Ornaghi, B.P., Meier, M.M., Lohbauer, U., Braga, R.R., 2014. Fracture toughness and cyclic

356   fatigue resistance of resin composites with different filler size distributions. Dent Mater 30,

357   742-751.

358   Randolph, L.D., Palin, W.M., Leloup, G., Leprince, J.G., 2016. Filler characteristics of modern

359   dental resin composites and their influence on physico-mechanical properties. Dental Materials

360   32, 1586-1599.

361   Ruse, N.D., Sadoun, M.J., 2014. Resin-composite blocks for dental CAD/CAM applications. J

362   Dent Res 93, 1232-1234.

363   Ruse, N.D., Troczynski, T., MacEntee, M.I., Feduik, D., 1996. Novel fracture toughness test

364   using a notchless triangular prism (NTP) specimen. J Biomed Mater Res 31, 457-463.

365   Takano, N., Fukasawa, K., Nishiyabu, K., 2010. Structural strength prediction for porous

366   titanium based on micro-stress concentration by micro-CT image-based multiscale simulation.

367   Int J Mech Sci 52, 229-235.

368   Takano, N., Zako, M., Kubo, F., Kimura, K., 2003. Microstructure-based stress analysis and

369   evaluation for porous ceramics by homogenization method with digital image-based modeling.

370   Int J Solids Struct 40, 1225-1242.

371   Tantbirojn, D., Versluis, A., Cheng, Y.S., Douglas, W.H., 2003. Fracture toughness and

372   microhardness of a composite: do they correlate? J Dent 31, 89-95.

373 Yamaguchi, S., Inoue, S., Sakai, T., Abe, T., Kitagawa, H., Imazato, S., 2017. Multi-scale

374 analysis of the effect of nano-filler particle diameter on the physical properties of CAD/CAM

375 composite resin blocks. Comput Methods Biomech Biomed Engin 20, 714-719.

376 Yamaguchi, S., Kani, R., Kawakami, K., Tsuji, M., Inoue, S., Lee, C., Kiba, W., Imazato, S.,

377 2018a. Fatigue behavior and crack initiation of CAD/CAM resin composite molar crowns. Dent

378 Mater 34, 1578-1584.

379 Yamaguchi, S., Mehdawi, I.M., Sakai, T., Abe, T., Inoue, S., Imazato, S., 2018b. In vitro/in

380 silico investigation of failure criteria to predict flexural strength of composite resins. Dent

381 Mater J 37, 152-156.

382 Yamaguchi, S., Tsutsui, K., Satake, K., Morikawa, S., Shirai, Y., Tanaka, H.T., 2014. Dynamic

383 analysis of a needle insertion for soft materials: Arbitrary Lagrangian-Eulerian-based three-

384 dimensional finite element analysis. Comput Biol Med 53, 42-47.

385 Yamanishi, Y., Yamaguchi, S., Imazato, S., Nakano, T., Yatani, H., 2014. Effects of the implant

386 design on peri-implant bone stress and abutment micromovement: three-dimensional finite

387 element analysis of original computer-aided design models. J Periodontol 85, e333-338.

388

389